Structural relaxations, vibrational dynamics and thermodynamics of vicinal surfaces

2003 J. Phys.: Condens. Matter 15 S3197

(http://iopscience.iop.org/0953-8984/15/47/002)

INSTITUTE OF PHYSICS PUBLISHING JOURNAL OF PHYSICS: CONDENSED MATTER

J. Phys.: Condens. Matter **15** (2003) S3197–S3226 PII: S0953-8984(03)67216-4

Structural relaxations, vibrational dynamics and thermodynamics of vicinal surfaces

Talat S Rahman[1], **Abdelkader Kara**[1] **and Sondan Durukanoğlu**[2]

[1] Department of Physics, Cardwell Hall, Kansas State University, Manhattan, KS 66506, USA
[2] Department of Physics, Istanbul Technical University, Maslak, 80626 Istanbul, Turkey

Received 5 August 2003
Published 14 November 2003
Online at stacks.iop.org/JPhysCM/15/S3197

Abstract

We present here a summary of the calculated structural, dynamical and thermodynamical properties of a number of vicinal surfaces of fcc metals with the aim of identifying trends in their characteristics. In general, multilayer relaxations indicate a contraction in the bonds between surface atoms except for that of the least undercoordinated surface atom ('corner') whose bond length with the nearest neighbour bulk atom displays an impressive expansion. Electronic structure calculations show a rearrangement of charge densities near the steps and the layer resolved density of states highlights the characteristics of the undercoordinated atoms. The frequencies of localized vibrational modes on stepped surfaces point to both softening and stiffening of specific force constants, which lead to enhancement of modes in both the lower and higher ends of the frequency spectrum in the vibrational densities of states. Contributions to the surface vibrational entropy from undercoordinated atoms are found to depend strongly on their atomic coordination and play an important role in determining the step excess free energy for certain step geometries. Comparisons of results are made with available experimental data.

(Some figures in this article are in colour only in the electronic version)

1. Introduction

In the past three decades of continuous advances in surface science techniques, stepped surfaces have acquired special significance for a number of reasons. In the 1970s, regularly stepped so called vicinal surfaces were used to probe zone boundary phonons [1] because experimental techniques such as electron energy loss spectroscopy (EELS) were in their infancy limited to measurements of modes present at the Brillouin zone (BZ) centre (Γ point). Since, by construction, the BZ for stepped surfaces involves the folding back of some zone boundaries to the zone centre, observations made at the latter part of the surface BZ could reveal modes with wavevectors corresponding to the former. It is in this spirit that Ibach and Bruchmann [1] measured phonons of stepped Pt[6(111) $\times$ (111)] using EELS. Techniques such as EELS

and He atom surface scattering have since become fully capable of measuring dispersion of surface phonons and have uncovered frequencies of step localized modes and their dispersion on vicinals of Cu [2, 3] and Ni [4]. Characteristics of step localized vibrational modes provide important information about the nature of the bonding between atoms in these regions of low coordination on stepped surfaces. There are, however, many other fundamental reasons for continued interest in their study. For some time now it has become clear that steps at surfaces provide favourable sites for chemical reactions and nucleation [5]. The role of steps in chemical reactions such as molecular dissociation has been the subject of intense recent study [6, 7]. As a result of undercoordination of step atoms, stepped surfaces are also subject to several types of structural change such as faceting, step doubling and roughening as a function of surface temperature and, in some cases, under the influence of adsorbates. There have thus been questions about the underpinnings of the reactivity and conditions of stability of vicinal surfaces.

In recent times, with increasing emphasis on nanoscience, vicinal surfaces have provided yet more reasons for their systematic study. To begin with, vicinal surfaces provide natural templates for the growth in nanostructures—a possibility already being exploited in the synthesis and examination of nanowires and magnetic nanostructures. Secondly, as a result of the variety of local environments of the surface atoms, vicinal surfaces provide a ready made atomic laboratory for examining the effect of local coordination and geometry on system characteristics. Depending on the extent of the local and/or extended nature of the chemical and physical properties of vicinal surfaces, the issue of their relevance to studies of nanoparticles can be addressed. As we will see, a number of features of vicinal surfaces, for a set of metals examined here, arise from local characteristics and open the way for making the connection to those of nanoparticles. Furthermore, steps are present on surfaces even when one least desires them. For processes such as epitaxial growth, self-assembly of molecular systems and other laboratory and industrial applications in which a solid surface serves as a template, the questions of the electronic, vibrational, thermodynamical characteristics of the steps on these surfaces become very much germane to the issues on hand. Vicinal surfaces, because of their regular (periodic) array of steps (which may or may not have kinks), provide a great avenue for controlled and systematic study of the role that steps can play wherever they may be present.

While the importance of stepped surfaces to many physical, chemical and engineering applications has been known of for sometime, more recent work exploits the chirality of kinked surfaces and their influence in distinguishing between the characteristic of self-assembly of molecules and the enantio-selectivity in chemical reactions [8, 9]. Given the multitude of areas of interest in understanding the characteristics of vicinal surfaces, the aim in this paper is to review some of the trends in behaviour, as a function of local geometry and terrace width. We have taken advantage of the fact that this volume contains contributions from a number of authors who have been pioneers in the field. We have thus restricted ourselves to considering vicinal surfaces which have been of most direct interest to us. These are the vicinals of several fcc transition metals for which we provide a review of the structural and dynamical properties and their contributions to the thermodynamical properties. The structural properties involve an analysis of multilayer relaxations, bond length changes of surface atoms and insights into the local electronic density of states, as a function of atomic coordination. By dynamical properties we mean here the features in the vibrational spectra of these surfaces whose origins and characteristics we trace. The aim here is to identify novel features which arise from the inherent complexity of these surfaces and the role that they play in the vibrational density of states. Reviewing the latter paves the way for presenting vibrational contributions to the entropy and free energy of the surfaces and the steps. These thermodynamical quantities are undoubtedly of great interest in considerations of the stability of the vicinal surfaces. Our

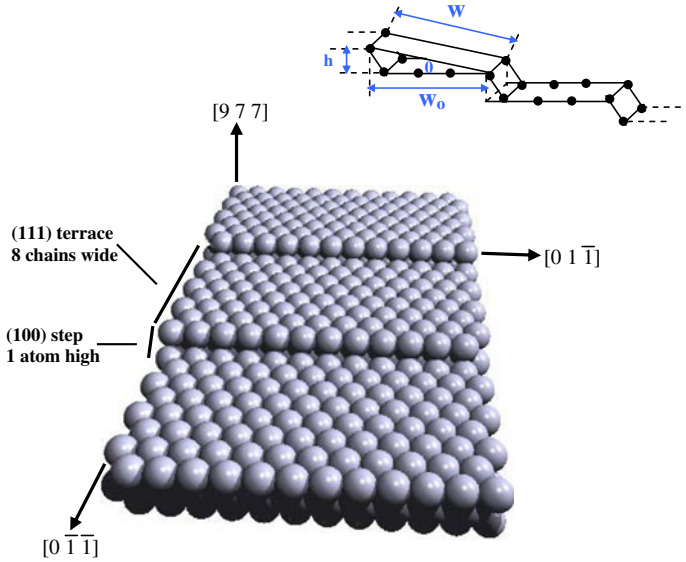

Figure 1. The hard sphere layout of a vicinal surface: fcc(977) is a vicinal of fcc(111) with a monatomic (100) microfaceted step face. The terrace is approximately eight atomic chains wide. The miscut angle θ and the terrace width w are shown in the inset.

purpose in this paper, however, is to identify the role that local coordination plays in controlling the characteristics and to establish whether vibrational contributions are so significant as to be non-negligible. We leave the question of relative stability and chemical reactivity of these surfaces for the future. While we made comparisons with experimental data where available, this paper mainly focuses on theoretical studies directed towards obtaining a microscopic understanding of the systems.

The rest of the paper is organized as follows. Section 2 contains a summary of the standard nomenclature used to identify vicinal surfaces with respect to the geometry of their terraces and step faces. This is followed in section 3 with a discussion of some of the theoretical techniques that are used. In section 4, a comparative analysis of the results is presented and compared with experimental data where available. Finally, conclusions regarding the trends in the behaviour and their correlation with local atomic coordination are summarized in section 5.

2. Surface nomenclature and geometry

Vicinal surfaces consist of regularly spaced low Miller index terraces separated by monatomic steps. They are obtained by cutting the crystal at an angle slightly off the low Miller index ((100), (111) and (110)) planes. Figure 1 is a hard sphere diagram of a fcc(977) surface showing the geometry of the terrace and the step face. In this case the terrace is an eight atom wide strip of fcc(111) surface, while the step face has a (100) microfacet. This vicinal is created by cutting the crystal at 7° away from the (111) plane towards the $[2\bar{1}\bar{1}]$ direction and compact, monatomic steps run along the $[0\bar{1}1]$ direction. On fcc(111) surfaces the $\langle 110 \rangle$ direction is not parallel to any plane of symmetry and there exist two different ways of generating monatomic stepped surfaces: by directing the miscut angle towards either the $[2\bar{1}\bar{1}]$ or the $[\bar{2}11]$ direction. In the case of the former, as we see in figure 1, the step face has a (100) microfacet (the so called A type), while in the case of the latter it would yield a (111) microfacet (the so called B type). The B type step corresponding to fcc(977) is fcc(997) for which the miscut angle is 6.5°.

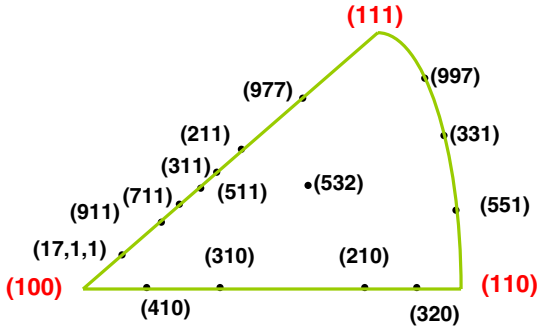

Figure 2. A stereographic projection for fcc crystals around the (100) pole showing several vicinal surfaces in relation to the low Miller index surfaces from which they are derived.

Table 1. Structural notation and geometric features for several fcc vicinals. Here d_b is the bulk interlayer separation, Δr is the surface registry and w is the terrace width (all in units of a, the lattice constant).

Miller index hkl	Compact-step notation $S(h_tk_tl_t) \times (h_sk_sl_s)$	Miscut angle (deg)	d_b (a)	Δr (a)	w (a)
311	2(100) × (111)	25.24	0.3015	0.6396	1.1726
511	3(100) × (111)	15.8	0.1924	0.680	1.8368
310	3(100) × (110)	18.44	0.1581	0.4743	1.581
410	4(100) × (110)	14.04	0.1212	0.4849	2.0616
211	3(111) × (100)	19.5	0.2041	0.5773	1.7319
977	8(111) × (100)	7.01	0.0747	0.6078	4.730
331	3(111) × (111)	22.0	0.2294	0.5677	1.5408
210	2(110) × (100)	26.56	0.2236	0.4472	1.118
320	3(110) × (100)	11.3	0.1387	0.6933	1.8026
551	3(110) × (111)	8.05	0.1400	0.9901	2.5247

A stereographic view of the collection of vicinals of varying terrace widths and geometries is shown in figure 2, drawn around the pole at fcc(100). The two types of vicinal for fcc(111) surfaces fall on the two sides of the graph around (111) separated by 60°. Together with (997) we have (331) which is also of B type with terrace widths of three atoms. The A type counterpart of (331) is (211) which lies on the same side of the stereograph as (977). For fcc(100) surfaces, the stereograph map neatly separates the two types of step face of its vicinals: those with a close packed (111) microfacet lie along the line joining the (100) pole to (111) and those with the (110) microfacet along the other line. An angle of 45° separates the in-plane orientation of these steps. Similarly, the set of loosely and close packed step faces of vicinals of fcc(110) flank the location of (110) on the stereograph with a separation of 90° between them. Thus along each side of the stereograph the terrace geometry and width change logically while maintaining the same geometry for the step face. In the Miller index notation, vicinals lying along the (100)–(110) side of the stereograph have indices $(hk0)$, while those along (110)–(111) have (hhk) and those along (111)–(100) are denoted by (hkk). A more self-explanatory notation for surface structure was introduced by Lang *et al* [10]. In this notation, the general form $S(h_tk_tl_t) \times (n_sk_sl_s)$ represents the Miller indices of the terrace plane $(n_tk_tl_t)$ and the step face $(n_sk_sl_s)$, respectively, and S is the atomic width of the terrace. In table 1 we summarize the notation for the various vicinal surfaces that are discussed in this paper, together with their miscut angles θ and the interatomic separations for ideal (bulk terminated)

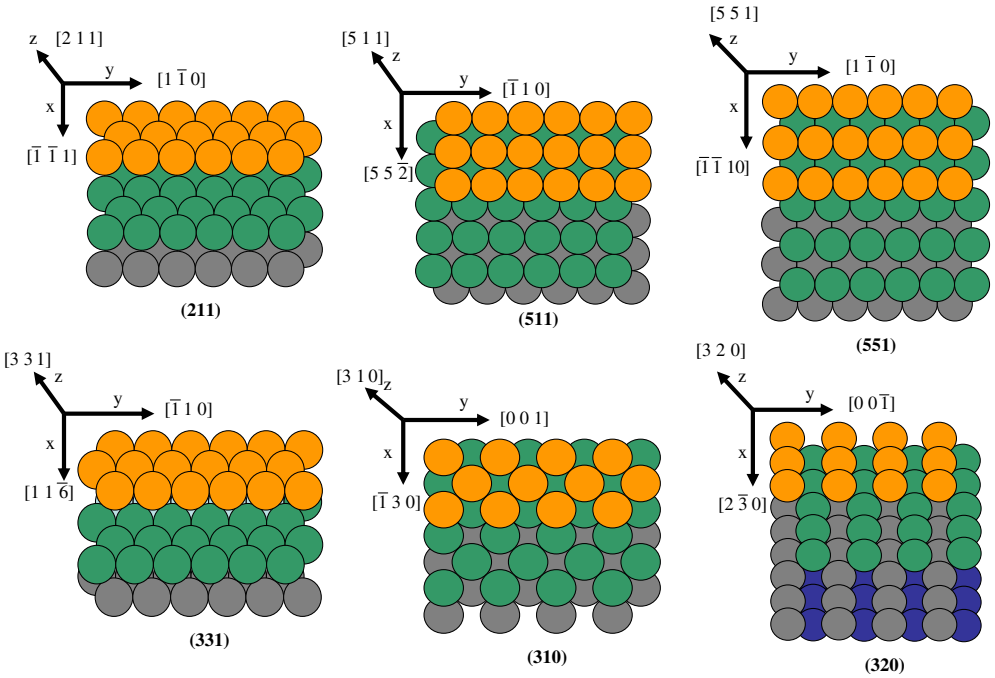

Figure 3. A top view of six vicinals of three atom wide terraces: (211) and (311) are vicinals of fcc(111); and (551) are vicinals of fcc(110).

geometry. Here w is the width of the terrace (see figure 1) and Δr is the registry (see figure 4). For comparative purposes we include in our list six vicinals, each of approximately three atom wide terraces, of the (100), (111) and (110) geometry and two types of step face as shown in the stereograph (figure 2). These six surfaces are shown in figure 3. Here (511) and (310) are vicinals of fcc(100), with (111) and (100) microfaceted step faces, respectively. The (310) is thus an open step arrangement and could be considered to be a regularly kinked step edge. The coordination of the step atoms is accordingly 6 for fcc(310). Next, the two corresponding surfaces of fcc(111) are (211) and (331) with the A and B types of step face, respectively. Finally, the corresponding surfaces of fcc(110) are (551) and (320), the former with a close packed (111) step face and the latter with a kinked (100) microfacet. In table 1, structural details of (311) and (210), which are vicinals of fcc(100) and fcc(110) with two atom wide terraces, are also provided. Details for (410) and (977) are given as well to provide the reader with a sense of the effect of increasing the terrace width. Quite clearly fcc(977) is just a broader terrace version of fcc(211) while (410) is related to (310). As in several previous studies [11, 12, 3, 13] we will use the following notation for the surface atoms, as illustrated in figure 4: SC for atoms in the step chain; TC for atoms in the terrace chain (if there is more than 1, we label them as TC1, TC2 etc) and CC for atoms in the corner chain. The coordination of these atoms on the six surfaces and the interatomic separation within a chain are summarized in table 2. For the three surfaces (310), (320) and (551), there are actually five undercoordinated sites—three in the top terrace and two underneath. In contrast, on (511), (211) and (331), there are only three undercoordinated sites. Together, these six surfaces provide a range of coordination from 6 to 11. The coordination of atoms on other vicinal surfaces can be found by extrapolation of those in table 2. An atom of great importance to us is labelled BNN in figure 4. This is the

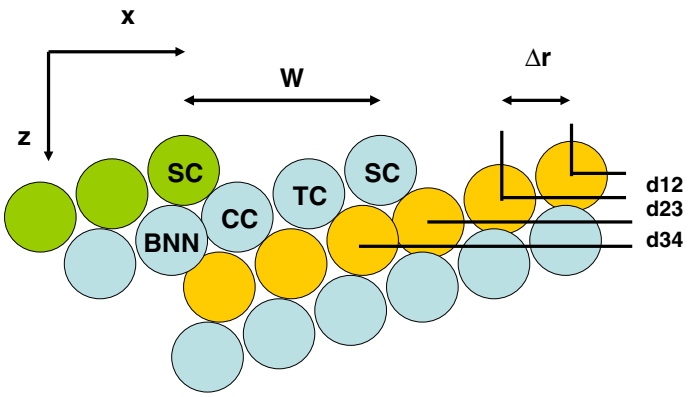

Figure 4. A side view of the vicinal surface showing the step (SC), terrace (TC), corner (CC) and BNN atoms, interlayer separations d_{ij} and surface registry (Δr).

Table 2. Atomic coordination and interatomic separation in the chains (Δy), where a is the lattice constant, for the six fcc vicinals.

Miller index	Δy	N_{SC}	N_{TC}	N_{CC}	N_{C4}	N_{C5}
511	$a/\sqrt{2}$	7	8	10	12	12
211	$a/\sqrt{2}$	7	9	10	12	12
331	$a/\sqrt{2}$	7	9	11	12	12
551	$a/\sqrt{2}$	7	7	9	11	11
320	a	6	7	9	11	11
310	a	6	8	9	11	12

nearest neighbour of the corner atom in the bulk and appears to participate in the electronic, structural and vibrational properties of the systems. In our calculations we have taken the x and y axes to lie in the surface plane, the x axis being perpendicular to the step and the y axis along the step. The z axis is along the surface normal.

3. Theoretical techniques

In this section we discuss some of the details of selected theoretical techniques which are used to calculate the structure, energetics, vibrational modes and densities of states, electronic charge densities and local electronic densities of states and also vibrational free energies of vicinal surfaces considered here. The section is divided into three parts dealing with calculations of (a) structure and energetics, (b) vibrational dynamics and (c) vibrational free energy. The review is by no means exhaustive and the details given are intended to motivate the reader to look up the original papers. As with any complex system, a range of theoretical and experimental techniques are applied to supplement the findings from the others. Since approximations are always involved, both in the extraction of information from experimental data and in the application of theoretical methods, it is the trend in the observed and calculated properties that is more meaningful than the quantitative information itself. It is thus interesting that for the systems considered here, despite the differences in theoretical techniques, the salient features in the characteristics are found to be very similar.

3.1. Determination of surface structure and energetics

Once the coordinates of atoms corresponding to the surface geometry discussed in table 1 are generated, it is necessary to allow the system to relax so that atoms find their equilibrium positions in their undercoordinated sites. Relaxations of atoms in the surface layers has been known of for quite some time, on both low and high Miller index surfaces. To obtain the relaxed position standard algorithms such as simulated annealing, steepest descent and conjugate gradient methods are used for minimizing the total energy of the system [14]. A critical ingredient in all such calculations is the interaction between the atoms/ion cores/electrons. One way to treat the system is to assume a particular form for the interatomic potential. In recent times semi-empirical many body potentials such as those from the embedded atom method (EAM) [15] and effective medium theory (EMT) [16] have been used. While such interaction potentials have had amazing success in predicting/explaining the characteristics of surfaces and nanostructures of six transition metals (Ni, Cu, Ag, Pd, Pt, Au), their reliability has to be checked by comparison with more accurate methods. Such an opportunity is provided by *ab initio* electronic structure calculations which have considerable predictive power and are becoming increasingly feasible even for complex systems such as surfaces with steps and kinks. Below we give some general details of *ab initio* electronic structure calculations that we and others have used. We follow this up with a short description of the EAM potentials which have been used to calculate structural properties of vicinal surfaces.

3.1.1. Ab initio electronic structure calculations. *Ab initio* electronic structure calculations have generally been performed within a pseudopotential approach to density functional theory (DFT) using either the local density approximation (LDA) [17] or the generalized gradient approximation (GGA) [18]. In [19] for example, the numerical implementation of the technique was based on a computer code developed by Meyer *et al* [20]. The LDA is applied using the Hedin–Lundqvist form of the exchange–correlation functional [21]. A norm conserving pseudopotential for Cu constructed according to a scheme proposed by Hamann *et al* [22] was used which has already been successfully employed for calculations of the structure and the phonons of low index surfaces of Cu [23]. A mixed basis set was then applied to represent the valence states consisting of five d type local functions at each Cu site, smoothly cut off at a radius of 2.3 au, and of plane waves with kinetic energy of 11 Ryd. The BZ integration was carried out using the special point sampling technique [24] together with a Gaussian broadening of the energy levels of 0.2 eV. For simulating surfaces the supercell consisted of 21–35 atoms (1 atom/layer), depending on the surface orientation. Structure optimization was carried out until the forces on all atoms were smaller than 10^{-3} Ryd au^{-1}, which is two orders of magnitude smaller than the forces present on the unrelaxed surfaces. Surface relaxations were found to be sensitive to the number of k-points used in the calculations. Sampling between 30 and 60 points in the BZ gave converged results.

In place of the mixed-basis representation, it is common to use *ab initio* DFT codes in which the Kohn–Sham equations are solved in a plane-wave basis. Codes such as the Vienna *ab initio* simulation package (VASP) [25] and those provided by the group of Norskov and Hammer [26] and Baroni *et al* [27] fall into this category. Typically, ultrasoft pseudopotentials of the Vanderbilt type [28] are used [29, 31, 32, 6], for which a cut-off energy for the plane-wave expansion of about 300 eV is found to give converged total energies for the system. BZ sampling using a Monkhorst–Pack mesh [24], together with a Methfessel–Paxton smearing [33] of the energy levels, produces reasonable results for Pd vicinals [29], for example. The Perdew–Wang functional [18] for the description of the exchange and correlation within the GGA is also invoked.

3.1.2. Many body interaction potentials. To describe the interactions between the atoms in model systems, several types of many body, semi-empirical potentials [15, 34, 16, 35] are currently being used. Because of its familiarity, we present here some details of the EAM developed by Foiles, Baskes and Daw. This is a semi-empirical, many body potential [15]. Although the EAM potentials neglect the large gradient in the charge density near the surface and use the atomic charge density for solids, for the six fcc metals Ag, Au, Cu, Ni, Pd and Pt, and their alloys, they do a good job of reproducing many of the characteristics of the bulk and the surface systems [15]. We find EAM potentials to be reliable for examining the temperature dependent structure and dynamics of Ag and Cu flat surfaces [36] and for describing the energetics of Cu vicinals and self-diffusion processes on the (100) surfaces of Ag, Cu and Ni [37, 38].

This method exploits the findings that:

(1) The ground state of an interacting electron gas is a unique functional of the total electron charge density [17].
(2) The energy of an impurity in a host is a functional of the electron density of the unperturbed host electron density [39].

That is, $E = F_{z,R}(\rho_{\mathrm{h}})$, where $\rho_{\mathrm{h}}(R)$ is the electron density of the host without impurity at R, the position where the impurity is to be replaced, and Z is the type of the impurity. Each atom in a solid is viewed as an impurity embedded in a host consisting of all other atoms and thus its energy is given by

$$E_i = F_i(\rho_i(R_i)) + \tfrac{1}{2}\sum_j \varphi(R_{ij}) \tag{1}$$

where ρ_i is the electron density of the host without atom i and is defined as a superposition of the f_j, the electron densities of atoms j as a function of distance from its centre:

$$\rho_i = \sum_{j\neq i} f_j(R_{ij}), \tag{2}$$

while R_{ij} is the distance between atoms i and j, $F_i(\rho_i)$ is the energy required to embed atom i in electron density ρ_i and φ is a short range electrostatic pair potential between atoms i and j. Hence, the total energy of a solid is simply a sum over all atoms in the solid and given by

$$E_{\mathrm{tot}} = \sum_i F_i(\rho_i(R_i)) + \tfrac{1}{2}\sum_{i,j} \varphi(R_{ij}). \tag{3}$$

It is further assumed that the electron density ρ_i is given by a linear superposition of the electron densities of the constituent atoms which is taken to be spherically symmetric. The EAM functions for the six fcc metals, Ag, Au, Cu, Ni, Pd and Pt and their alloys were developed by numerically fitting the functions to the bulk lattice constants, cohesive energy, elastic constants, vacancy formation energy and alloy heats of mixing. Using these interactions for a model system constructed in its bulk terminated positions, the conjugate gradient method is used to relax the system to 0 K equilibrium configuration. The dynamical matrix needed to calculate the vibrational (or phonon) density of states for a system of interest is then obtained from analytical expressions for the partial second derivatives of the EAM potentials [15].

3.2. Determination of the vibrational density of states

There are several theoretical techniques for calculations for surface and bulk phonons in crystals. The most commonly used is the slab method in which one needs to diagonalize the dynamical matrix portraying the interactions between the particles in N layers of the slab [40].

In the case of high Miller index surfaces, in particular vicinal surfaces with large terraces, representative of large surface periodicities, slab calculations are hampered by the need for huge slabs to describe the complexity of the surface structure. The continued fraction (CF) method using a real space Green function is another way to proceed [41]. In this method the surface matrix is treated as a perturbation to the bulk and the surface Green function is obtained by projecting the bulk Green function into the subspace defined by the perturbation matrix. Both slab and CF methods are developed in wavevector space. If the interest lies in gaining insight into the local contributions to the dynamics and thermodynamics of systems possessing site specific environments, a local approach in real space is perhaps more useful than one based on k-space. The real space Green function (RSGF) method is one such method [42]. Instead of wavevectors and BZs, one can focus on any 'local' region and analyse the effect of the rest of the system on it. Since it does not require the system to be periodic, it is particularly suitable for studying local vibrational densities of states in complex systems with defects and disorder. The only prerequisite is that the interatomic potential between the atoms in the system be of finite range, so that one can write the force constant matrix in a block-tridiagonal form. There is also no *a priori* truncation in the system size, as would be the case for the matrix diagonalization methods based on k-space. The real space Green function method also has an advantage over the familiar 'CF' method [41] as it does not involve truncation schemes to determine the recursion coefficients; rather, a more general and simpler recursive scheme is applied.

The first step in the application of RSGF method is to divide the system (with a finite interaction range) into regions such that the Hamiltonian can be written in a block-tridiagonal matrix as follows:

$$H = \begin{pmatrix} \ddots & & & & \\ v_{i,i-1} & h_i & v_{i,i+1} & & \\ & v_{i+1,i} & h_{i+1} & v_{i+1,i+2} & \\ & & & \ddots & \end{pmatrix}, \tag{4}$$

where the sub-matrices h_i along the diagonals are $(3n_i \times 3n_i)$ square matrices and the sub-matrices $v_{i,i+1}$ along the 'off-diagonals' are matrices of dimension $3n_i \times 3n_{i+1}$ with n being the number of particles in the locality. The Green function associated with the matrix H is given by

$$G(z) = (zI - H)^{-1} \tag{5}$$

where $z = w^2 + \mathrm{i}\varepsilon$, ε being the width of the Lorentzian representing the delta function at w^2, and I is a unit matrix of the same size as H.

The diagonal elements of the Green function matrix which lead to the local Green function matrix corresponding to any chosen locality are given by [42]

$$G_{ii} = [(zI - h_i) - v_{i,i+1}\Delta^{+}_{i+1}v_{i+1,i} - v_{i,i-1}\Delta^{-}_{i-1}v_{i-1,i}]^{-1}. \tag{6}$$

(Δ^{+}_i) and (Δ^{-}_i) are defined as forward and backward partial Green functions and described by

$$\Delta^{+}_i = (zI - h_i - v_{i,i+1}\Delta^{+}_{i+1}v_{i+1,i})^{-1}, \tag{7}$$

$$\Delta^{-}_i = (zI - h_i - v_{i,i-1}\Delta^{-}_{i-1}v_{i-1,i})^{-1}. \tag{8}$$

The relation between the diagonal elements of the Green function matrix G is [42]

$$G_{ii} = \Delta^{\pm}_i + \Delta^{\pm}_i v_{i,i\mp1}G_{i\mp1,i\mp1}v_{i\mp1,i}\Delta^{\pm}_i. \tag{9}$$

As seen in the above equations, in the method of the resolvent matrix, the calculation of Green functions is reduced to a series of inversions and multiplications of matrices whose dimensions are usually much smaller than the total degree of the system under consideration. Another

feature of the method is that one can focus on any specified locality in the system and calculate the corresponding Green function, a diagonal element of the Green function representing the entire system. This can be achieved through the forward and backward partial Green function matrices $\Delta_i^{\pm}$ (see equation (9)).

In this paper the real space Green function is used to calculate the local vibrational density of states through a layer-by-layer approach in which an infinite system with some periodicities is viewed as a stack of two dimensional atomic layers, stacked upon one another, along some crystal axis. Hence, the elements of the sub-matrices in the block-tridiagonal matrix describe the force constants between the particles within and between the associated localities containing a certain number of two dimensional atomic layers [43].

The normalized vibrational density of states is given by the function

$$g(\omega^2) = -\frac{1}{3n\pi} \lim_{\epsilon \to 0} \mathrm{Im}\,\mathrm{Tr}[G(\omega^2 + \mathrm{i}\epsilon)]. \tag{10}$$

The frequency dependent vibrational density of states $N(\omega)$ follows directly from

$$N(\omega) = 2\omega g(\omega^2). \tag{11}$$

3.3. Determination of vibrational free energy

In a set of studies we have employed the harmonic approximation of lattice dynamics to calculate the local and excess vibrational free energy for vicinal surfaces of interest [11–13, 44]. We expect the results summarized here to be valid for low temperatures, which for vicinals of Cu and Ag surfaces would be up to 500 K. The main quantity of interest here is the vibrational contribution to the free energy of the stepped surfaces. While details of the calculations may be found in [12], we include the main points here.

The free energy of a system is given by the standard definition $F = U - TS$, where U is the internal energy, S is the entropy and T is the temperature. Both U and S have contributions from atomic configurations and vibrations, such that $F = F^{\mathrm{conf}} + F^{\mathrm{vib}}$. That is, for each atomic configuration of the system there is a specific vibrational contribution, which can be further written as $F^{\mathrm{vib}} = U^{\mathrm{vib}} - TS^{\mathrm{vib}}$. It is this latter quantity that we calculate here for the five surface systems of interest, for their relaxed atomic configurations (of minimum energy) at 0 K. In the harmonic approximation, the free energy is given by

$$F^{\mathrm{vib}} = k_{\mathrm{B}}T \int_0^{\infty} \ln\left(2\sinh\left(\frac{x}{2}\right)\right) N(\nu)\,\mathrm{d}\nu. \tag{12}$$

Here $x = h\nu/k_{\mathrm{B}}T$ and $N(\nu)$ is the vibrational density of states (as a function of frequency ν) which can be written as $N(\nu) = \sum_l n_l(\nu)$, where $n_l(\nu)$ is the local density of states (LDOS) of atoms in layer l.

To calculate the vibrational contribution to the free energy of a surface (flat, stepped, kinked, ...) we consider a slab of N atoms, arranged such that the top and bottom surfaces consist of the Miller index planes. The surface free energy, which is defined as the excess over the values associated with the bulk system, is evaluated using the following expression:

$$F_{\mathrm{SUR}}^{\mathrm{vib}} = (F_{\mathrm{SLAB}}^{\mathrm{vib}} - NF_{\mathrm{BULK}}^{\mathrm{vib}})/(2A). \tag{13}$$

In the above equation, $F_{\mathrm{SLAB}}^{\mathrm{vib}}$ and $F_{\mathrm{BULK}}^{\mathrm{vib}}$ are, respectively, the vibrational free energy calculated for a finite slab representing the surface system and a single bulk atom; A is the surface area of the system. The factor 2 arises from the fact that the system contains two free surfaces.

In the same vein, the step vibrational energy is defined as the excess energy over that for a flat surface of the same geometry as the terrace. The vibrational contribution to the step free energy is then calculated using the following equation [45]:

$$F_{\mathrm{STEP}}^{\mathrm{vib}} = F_{\mathrm{S}}^{\mathrm{vib}}(\theta) - (p - 1 + f)F_{\mathrm{S}}^{\mathrm{vib}}(\infty), \tag{14}$$

Table 3. Experimental data on the relaxation of metal vicinal surfaces as changes from the bulk separation (in %).

Surface	Experiment	Δd_{12}	Δd_{23}	Δd_{34}	Δd_{45}	Δd_{56}	Δd_{67}	Δd_{78}	Δd_{89}
Cu(311)	LEED [58]	−7.3	+3.7	0.0					
Cu(311)	LEED [59]	−11.9	+1.8						
Cu(511)	X-ray [51]	−15.4	+8.1	−1.1	−10.3	+5.4	−0.7	−6.9	+3.6
Cu(511)	LEED [50]	−13.2	−6.1	+5.2	−0.1	+2.7			
Cu(211)	LEED [60]	−14.9	−10.8	+8.1					
Cu(331)	LEED [47]	−13.8	+0.4	+4.0	−4.0				
Cu(711)	LEED [52]	−13	−2	−10	+7	−1	−4	+7	
Cu(320)	QLEED [61]	−24	−16	+10					
Cu(210)	LEED [62]	−11.12	−5.68	+3.83	+0.06	−0.66			
Pt(210)	LEED [63]	−23	−12	+4	−3				
Al(210)	LEED [64]	−16	−1	+9	−4	−1			
Al(311)	LEED [65]	−13	+9						
Al(331)	LEED [66]	−11.7	−4.1	+10.3	−4.8				
Ni(311)	LEED [67]	−15.9	+4.1	−1.6					
Ag(410)	LEED [46]	0	−36	+18					
Pd(210)	LEED [68]	−3	+7	+3	−1				
Pd(320)	LEED [69]	−15	−9	−6	+15	+6			

where $F_{\mathrm{STEP}}^{\mathrm{vib}}$ is the vibrational step free energy, $F_{\mathrm{S}}^{\mathrm{vib}}(\theta)$ and $F_{\mathrm{S}}^{\mathrm{vib}}(\infty)$ are the vibrational surface energies corresponding the vicinal and the flat surface forming the terraces of the vicinal surface and p is the number of atomic chains on the terrace. f is a geometrical factor determined by the projection of the ledge on the terrace and it is $2/3$ for (211), $1/3$ for (331) and $1/2$ for (511). The vibrational surface free energies in the above equation, as the excess energies over the bulk, are calculated using

$$F_{\mathrm{S}}^{\mathrm{vib}} = \sum_{i}^{n} F_{i}^{\mathrm{vib}} - F_{\mathrm{b}}^{\mathrm{vib}}, \tag{15}$$

where F_{i}^{vib} and $F_{\mathrm{b}}^{\mathrm{vib}}$ are the vibrational free energies for the atoms in layer i and in the bulk and calculated using equation (1) with the local density of states associated with the layer of interest.

4. Results

4.1. Multilayer relaxations

In tables 3–5, we have summarized the calculated and observed relaxation patterns of vicinals of fcc transition metals that we are aware of. The list is by no means complete and entries are not available for every transition metal of interest. Most of the work appears to be on Cu and Pd surfaces with a few studies on Ag, Ni, Al and Pt. The surface geometries and step face orientations of ten of them have been summarized in table 1. The geometry of the others is related to those of the basic six illustrated in figure 3 except for the number of atoms in the terrace. Thus (711), (911), (11 1 1) and (17 1 1) are vicinals of fcc(100) with four, five, six and nine atoms on each terrace and (111) step face with the notation $(2n - 1\,1\,1)$. On the other hand, (510), (710) and (910) have (100) terraces of five, six and nine atoms, respectively, with a (110) microfaceted step face. Similarly, (430) has a four atom wide (110) terrace with a (100) microfaceted step face. To avoid confusion we have summarized the experimental data

Table 4. First principles calculations of the relaxation of metal vicinal surfaces as changes from the bulk separation (in %).

Surface	Method	Δd_{12}	Δd_{23}	Δd_{34}	Δd_{45}	Δd_{56}	Δd_{67}	Δd_{78}	Δd_{89}
Cu(311)	PPPW [31]	−15.0	+4.0	−0.6	−1.1	+0.4	−0.7	0.0	
Cu(511)	PPPW [19]	−9.3	−10.7	+7.2	−2.9	+1.1	+1.7	−1.5	+1.6
Cu(511)	PPPW [31]	−11.1	−16.4	+8.4	−4.6	+2.3	−1.5	+0.2	+0.8
Cu(711)	PPPW [19]	−7.3	−1.5	−14.8	+8.0	−1.0	−1.1	+1.4	+1.7
Cu(711)	PPPW [31]	−9.3	−7.7	−21.8	+14.3	−3.0	−9.1	+5.6	−0.2
Cu(911)	PPPW [19]	−11.2	−2.2	+0.6	−13.9	+5.4	−1.3	−4.1	+4.5
Cu(911)	PPPW [31]	−7.4	+0.8	−10.5	−23.3	+25.9	−0.5	−4.1	−10.5
Cu(1 1 11)	PPPW [31]	−8.3	−2.7	−1.7	−10.7	−19.9	+26.3	+1.9	−4.0
Cu(211)	PPPW [19]	−12.2	−9.5	+8.7	−2.1	−1.6	+1.5	−0.1	−0.3
Cu(211)	PPPW [70]	−14.4	−10.7	+10.9	−3.8	−2.3	+1.7	−1.0	−0.05
Cu(211)	FLAPW [71]	−28.4	−3.0	+15.3	−6.6	+0.7	+3.0		
Cu(331)	PPPW [19]	−12.7	−3.3	+4.9	−2.0	+0.1	−0.1	+0.8	−0.6
Cu(331)	FLAPW [71]	−22.0	+1.6	+6.9	−2.4	−0.6	−0.4		
Cu(210)	PPPW [30]	−13.4	−6.2	+5.3	+0.6	−1.7	−0.9	+0.6	
Cu(510)	PPPW [31]	−9.2	−6.4	−2.8	−21.8	−7.3	+20.4	−1.7	−6.2
Cu(710)	PPPW [31]	−15.6	−8.4	−3.2	−9.0	−10.3	−20.1	+0.5	+24.5
Cu(910)	PPPW [31]	−15.5	−8.9	−11.1	−0.1	−4.4	+6.1	+10.1	−33.2
Pd(210)	PPPW [32]	−17	−3	+10	−4				
Pd(211)	PPPW [29]	−12.3	−13.0	+17.4	−6.1	−2.0	+3.6	−2.7	0.0
Pd(331)	PPPW [29]	−12.0	−7.7	+10.9	−4.8	+0.2			
Pd(320)	PPPW [29]	−15.5	−18.0	+1.8	−11.6	+22.8	−8.2	−3.1	+6.3
Pd(320)	PPPW [30]	−11.9	−19.2	−0.6	−5.9	+16.8	−4.5	−3.2	
Pd(551)	PPPW [29]	−8.8	−15.7	−3.4	−6.5	+18.5	−6.9	−1.7	+2.8
Al(331)	CP [72]	−11.3	−6.3	+10.1	−4.4	−1.8	+4.8		

Table 5. Relaxation of metal vicinal surfaces as changes from the bulk separation (in %) obtained using model potentials.

Surface	Method	Δd_{12}	Δd_{23}	Δd_{34}	Δd_{45}	Δd_{56}	Δd_{67}	Δd_{78}	Δd_{89}
Cu(311)	EAM [73]	−8.9	+3.8	−3.6	+2.0	−1.3			
Cu(311)	EMT [74]	−6.6	+3.1	−2.9	+1.5	−1.0			
Cu(511)	EAM [75]	−8.9	−7.2	+8.3	−3.8	−3.6	+4.6	−1.6	−1.5
Cu(711)	EAM [75]	−10.0	−5.3	−9.7	+13.8	−4.5	−4.5	−4.6	+3.0
Cu(11 1 1)	EAM [75]	−14.1	−3.8	−3.7	−6.2	−12.5	+23.9	−5.1	−3.3
Cu(310)	EAM [75]	−11.9	−10.3	+2.9	+5.5	−3.9	−3.7	+4.2	+2.0
Cu(211)	EAM [75]	−9.8	−4.8	+6.9	−5.2	−1.0	+3.7	−2.4	−0.2
Cu(331)	EAM [75]	−9.9	+1.8	−1.5	−0.2	−0.3	+0.5	−0.4	+0.1
Cu(551)	EAM [75]	−5.4	−11.9	+6.0	−7.2	+3.1	+1.3	−4.4	+2.6
Cu(410)	EAM [53]	−12.7	−8.7	−11.6	+6.2	+9.2	−4.6	−5.5	−3.6
Cu(320)	EAM [44]	−13.1	−9.0	+3.1	−8.1	+10.0	−5.5	−1.6	+3.0
Ag(320)	EAM [76]	−9.8	−10.4	+1.1	−5.9	+7.0	−3.3	−1.8	+2.8
Ag(410)	EAM [44]	−11.6	−5.3	−9.9	+2.1	+6.7	−3.9	−3.7	
Ni(320)	EAM [76]	−9.0	−5.4	+2.8	−5.1	+6.4	−3.7	−0.7	+2.0
Pd(320)	EAM [76]	−20.3	−19.3	−0.6	−14.0	+18.3	−8.8	−3.8	+6.1
Pd(430)	EAM [76]	−22.7	−9.3	−24.4	+2.2	−10.8	−13.6	+28.7	−8.1

in table 3, the theoretical results from *ab initio* calculations in table 4 and those from EAM potentials in table 5. A number of the surfaces reported in tables 4 and 5 have been studied by several groups using related techniques; where possible we have given references to these

papers. In general we have not found significant deviation in the results, except for one case which we will mention below.

A quick glance at table 3 confirms that for the entire set of transition metals for which experimental data are available, the step atoms move inwards by a noticeable amount. The Δd_{ij} in the table are the deviations (in %) of the separation between atoms in layers i and j from the spacing in the bulk. The labellings of the layers and the interlayer separations Δd_{ij} are illustrated in figure 4. With a few exceptions the experimental values of the inward relaxations of the step atoms on these surfaces are about 12%–15%. This estimate is approximate since experimental data contain an error bar of about 4%. Nevertheless, the uniformity of the results is striking. It is also clear from table 3 that atoms other than those at the step may also undergo impressive relaxations and that for some atoms the relaxation is outwards. We should note that the experimental values of relaxations for Ag(410) appear to be anomalous. Apparently there were some problems in the analysis of the data [46] because of the uncertainties in measuring small changes in bond lengths from an earlier LEED analysis program. Although this situation has improved considerably with the newer versions of the programs [47], extraction of multilayer relaxations from experimental data is a daunting task. It is thus impressive that experiments are able to detect spacing changes for several layers into the bulk, as is the case for Cu(511) and Cu(711), from very detailed low energy electron diffraction (LEED) analysis. For surfaces in table 3 for which results are available for only the top two or three layers, it is difficult to predict a pattern.

A better sense of the trends in the multilayer relaxations is perhaps obtained from examining the entries in tables 4 and 5 which have been obtained from calculations. For all surfaces considered, regardless of the terrace width and whether *ab initio* methods or model interaction potentials were used, the step atoms undergo a significant inward relaxation. There is also broad quantitative agreement between the results obtained from *ab initio* calculations, model potentials and experimental data for relaxations of the step atoms, with one exception. It is not clear to us why the full potential linear augmented plane-wave method (FLAPW) gives results for the relaxations of the step atoms of Cu(211) and Cu(331) that are so different from those from the pseudopotential plane-wave (PPPW) method and experimental data. We are in the process of repeating these calculations to locate the reason for these differences. Nevertheless, the trends in the multilayer relaxations from the FLAPW method are very similar to those from other methods. All calculations in tables 4 and 5 show the relaxations on stepped Cu, Pd, Al, Ni and Ag to persist on all surfaces for a large number of layers. Of course, the concept of layers is different here from that for flat surfaces (see figure 4). The first n layers, for example, are all exposed to the vacuum, where n is the number of atoms on the terrace. Correspondingly, the interlayer separations are small and even large percentage changes in interlayer separations correspond to small numbers in distances. It is important to bear this point in mind when comparing the results for a particular surface either with those for flat surfaces or with the results from other methods.

A common feature of all surfaces examined in table 4 is that all terrace atoms except for the ones in the corner chain (CC) undergo significantly large inwards relaxations. The corner atoms are always found to relax outwards. Additionally, the atoms in the terrace adjacent to CC exhibit comparatively large inward relaxations whose magnitude maybe larger than that for the step atoms (SC). For example, for Cu(511), Cu(711) and Cu(911), the changes, respectively, in d_{23} (involving TC1), d_{34} (involving TC2) and d_{45} (involving TC3) are larger than that of d_{12}. These trends are in qualitative agreement with LEED data on Cu(511) and Cu(711) and with Schmolkowski's [48] ideas of charge smoothing, such that the maximum relative change in interlayer separation is focused around the corner atoms. The situation with the more close packed surface Cu(331) is somewhat different. In figure 5 we have plotted

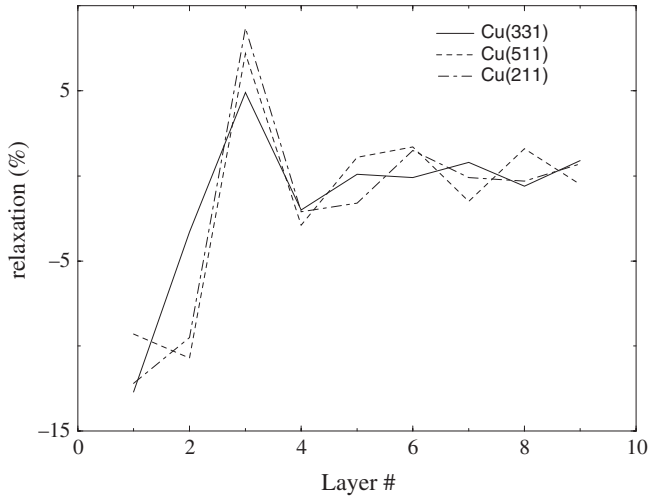

Figure 5. The relaxation patterns for Cu(331), Cu(511) and Cu(211) show the effect of a small difference in the local geometry.

the relaxation patterns for Cu(331), Cu(511) and Cu(211) to show the influence of the local coordination of Cu(331) on its relaxation pattern. The change in Δd_{23} is much smaller on Cu(331) than on the other two surfaces.

While the predicted relaxation patterns for Cu surfaces from *ab initio* electronic structure calculations are in reasonable agreement with those from semi-empirical potentials, there is a remarkable difference. An intriguing result for multilayer relaxations of the vicinals of Cu(100) obtained with EAM potentials in [37] was that the pattern of inward and outward relaxations continued well into the bulk with an exponentially decreasing amplitude, as shown very nicely for Cu(17 1 1) in figure 6. Tian and Rahman [37] found this oscillating behaviour and decay to be characteristic of a set of vicinals of Cu(100). Since for Cu(711) we also have experimental data available, it is worthwhile to compare the pattern obtained from EAM potentials and *ab initio* calculations for this surface. The relaxation pattern predicted by EAM is $(-\,-\,-+,\,-\,-\,-+,\,-\,-\,-+,\ldots)$ with an eventual damping of the relaxations. The pattern for Cu(711) from table 4 is instead $(-\,-\,-+,\,-\,-+\,+,\,-\,-\,+\,+)$ and does not reflect a decaying amplitude as we move into the bulk. Furthermore, the *ab initio* result is more in agreement with experimental data. A long time back Allan [49] also predicted an oscillatory, damped relaxation of atoms at surfaces on the physical basis of charge oscillations in crystals. It is thus surprising that this interesting result is not corroborated by experiment and *ab initio* calculations. Since there is a good margin for error in each analysis, it would be interesting to look at data for other surfaces when they become available, to achieve further understanding.

The *ab initio* results for Pd surfaces in table 3 obtained by Makkonen *et al* [29] also display very similar behaviour to their Cu counterparts. The results for Pd(320) and Pd(551) provide an even stronger argument for the association of the outward relaxation with that of the least undercoordinated surface atom. Because of the open structure of the fcc(110) terraces of these two surfaces, it is the atom in the fifth layer (with the layers defined as for vicinal surfaces (figure 4)) with coordination number 11 that is the last one exposed to the vacuum. These atoms are thus forced to move outwards so as to smooth the charge density on the terrace. This particular result is further corroborated by the results from EAM potentials on several vicinals of Pd(110), Cu(110), Ag(110) and Ni(110). For such vicinals with three atom wide terraces,

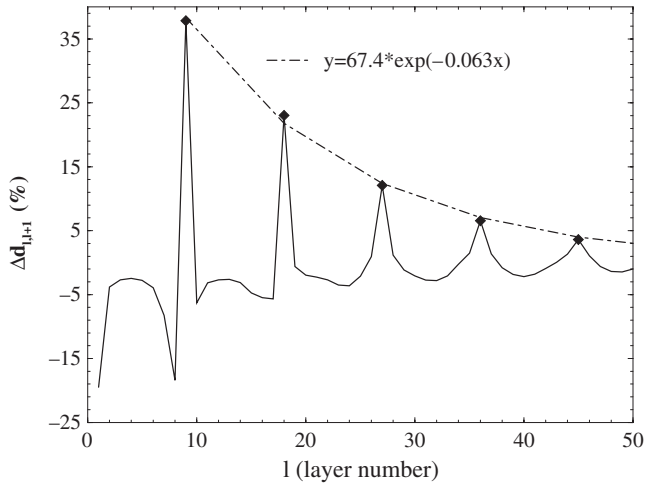

Figure 6. Multilayer relaxation of Cu(17 1 1) showing the oscillatory nature of the relaxation pattern and the damping of its amplitude (courtesy Z Tian and T S Rahman).

the most prominent outward relaxation is found for Δd_{56}. On the other hand, for vicinals of Cu(111), Cu(100), Al(111), Pd(100) and Pd(111) with three atom wide terraces, impressive outward relaxation appears for Δd_{34}. For vicinals of fcc(100), the outward relaxations of d_{45} for Cu(711), d_{56} for Cu(911) and d_{67} for Cu(11 1 1) from *ab initio* calculations (table 4) and EAM potentials (table 5) also point to an interesting characteristic of the least undercoordinated surface atom. Calculations of relaxations of Cu(311) and Cu(210), in table 4, each with a two atom wide terrace, of fcc(100) and fcc(110) geometry, with outward relaxations of d_{23} and d_{34}, respectively, provide the same conclusion. Multilayer relaxations of Pd(430), a vicinal of Pd(110) with a four atom wide terrace, in table 5, indicate outward relaxation for d_{78} which is once again that for the least undercoordinated surface atom.

We now turn to a comparison of the theoretical results in tables 4 and 5 with the experimental ones in table 3. For Cu(311) there appears to be excellent agreement between data and theoretical results. First principles calculations suggest a larger inward relaxation of the step atom than concluded from the analysis of experimental data. However, given the uncertainties in determining changes in these small distances, the qualitative agreement between two sets of data and both types of calculation for Cu(311) is remarkable. Experimental data on Al(311) and Ni(311) show a very similar trend in behaviour to Cu(311). While calculations are not yet available for these two surfaces, it is unlikely that they will be in qualitative disagreement with the data. Turning to the relaxations of vicinals of Cu(111) of the A and B types, experimental and theoretical results for both Cu(211) and Cu(331) are in general overall agreement, apart from quantitative differences between results from FLAPW calculations and the others, as already mentioned. The slight discrepancy in the results for LEED data for d_{23} and calculations may also be ignored because of the error margin of 4% in the analysis of the data and a similar one among the different types of calculation. LEED data on Al(331), in table 3, display a very similar trend to those for Cu(331) and are in excellent agreement with the results of *ab initio* calculations in table 4.

The case of multilayer relaxations for Cu(511) is interesting because of the differences between published data from LEED [50] and x-ray measurements [51]. Except for the displacement of the step atoms, for which all results point to a large inward relaxation, the results from

x-ray scattering measurements are in disagreement with theoretical results and with those from LEED. We do not understand the reasons for this disagreement. It should be noted that the differences from the x-ray results are both qualitative and quantitative, beyond the established error bars in the experiments and calculations.

Comparison of theoretical results for Cu(711) with those in table 3 from LEED data shows that the *ab initio* results are in excellent agreement with the data and that the small differences from the EAM results that the authors [52] had noted is removed. As in the case of Cu(511), the largest percentage change in the interlayer spacing is not for d_{12}. In this case it is for d_{34} which separates CC from TC2. As before, there is outward relaxation of the spacing between CC and BNN. The fact that relaxations near CC remain strong even as the terrace width increases is interesting in itself.

The recently obtained data on the relaxations of Cu(210) (table 3) surfaces have now been shown to be in excellent agreement with results from *ab initio* calculations (table 4). The trend $(- - +)$ for the relaxation of the top three layers is borne out in the LEED data for Pt(210) and Al(210), shown in table 3. Similarly the QLEED results for relaxations of Cu(320) are qualitatively reflected in EAM calculations in table 5.

This brings us to a discussion of the experimental results for vicinals of Pd(110). For both Pd(210) and Pd(320), the experimental data are not in full agreement with results of *ab initio* calculations (or those from EAM potentials). The trend for Pd(210) is reported to be $(- + +)$ in LEED data, in table 3, and $(- - +)$ in *ab initio* calculations. Since experimental data on Pt(210), Al(210) and Cu(210) exhibit the trend $(- - +)$, we suggest that the LEED data on Pd(210) be re-examined. It could be that the difference in theoretical and experimental values comes from an assumption in the data analysis. Similar is the case for Pd(320) for which two sets of *ab initio* calculations and those from EAM potentials show the trend $(- - + - + -)$ while LEED data reveal the oscillation to be $(- - - + +)$. In figure 7, we have plotted the relaxation patterns for the (320) surfaces of Pd, Cu, Ag and Ni, using EAM potentials. The trend is undoubtedly the same; i.e., the strongest outward relaxation is that of the fifth layer atom. It would thus be helpful to have a re-examination of the LEED data for Pd(320). In table 5, we have also included the relaxations for Pd(430) which also displays the same trend as shown in theoretical results for all the surfaces considered so far—namely, the striking outward relaxation is that of the least undercoordinated surface atom. In the case of Pd(430) this is the atom in the seventh layer.

Unlike flat surfaces, vicinal surfaces relax in both x and z directions, since the existence of steps at the surface leads to broken symmetry in both of these directions. While relaxations along the z direction yield characteristic interlayer separations that we have discussed above, those along the x direction provide new registries of atoms, as compared to those in the bulk. Our percentage intralayer registries from *ab initio* calculations of several surfaces are summarized in table 6. As in the observations from EAM calculations [53], the changes in the registries of the atoms are small. However, the changes in registries of the atoms are not inconsequential since they affect the changes in the bond lengths between the atoms in these regions of low coordinations. In table 7, we tabulate results for the total changes in the distances between the step atoms and their nearest neighbours for some surfaces. For comparison we include results from *ab initio* calculations and EAM potentials (in parentheses). The largest changes in the bond lengths are for those between the step atoms and their bulk nearest neighbour (BNN) which lies right below them. The bonds between CC and the BNN show small enlargement, while all other bonds in table 7 are found to undergo shortening. A plot of the changes in the bond lengths, in figure 8, between SC and its nearest neighbours for Cu(711), Cu(911) and Cu(17 1 1) shows that the effect is independent of the terrace width and thus is local.

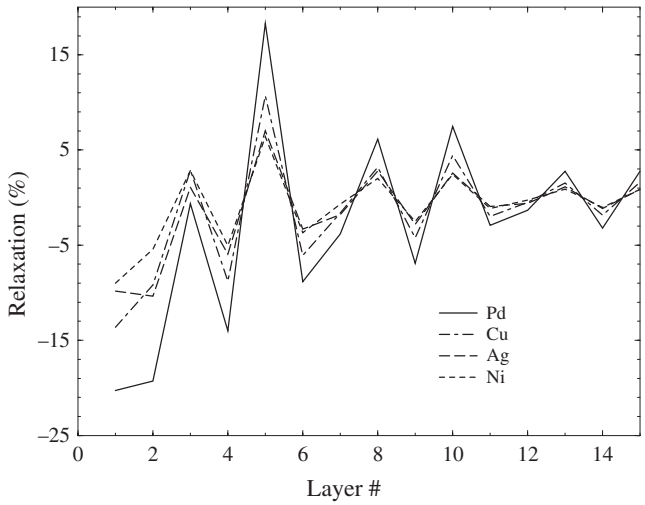

Figure 7. Multilayer relaxation of the (320) surface for Pd, Cu, Ag and Ni showing the generality of the relaxation pattern.

Table 6. Calculated changes in the registries as percentages of that for the ideal surface r_b (in %).

Registry	Cu(211) [19]	Cu(331) [19]	Cu(511) [19]	Cu(711) [19]	Cu(911) [19]	Cu(210) [30]
r_b	2.083 Å	2.048 Å	2.454 Å	2.500 Å	2.519 Å	1.644 Å
r_{12}	−1.22	−0.10	−1.17	−1.37	+0.99	−0.84
r_{23}	−0.54	−1.74	−1.21	−0.32	−0.40	−1.17
r_{34}	−0.22	+1.46	+0.98	−0.41	+0.28	+1.96
r_{45}	+1.50	+0.62	+0.25	+0.77	−0.60	+0.02
r_{56}	−0.26	−0.50	−0.31	+0.23	+0.38	−0.50
r_{67}	+0.19	+0.24	+0.01	+0.82	−0.01	−0.02
r_{78}	0.00	−0.19	0.00	−0.89	+0.55	
r_{89}	−0.11	+0.23	−0.14	−0.01	+0.16	
$r_{9,10}$				−0.31	−0.44	
$r_{10,11}$				−0.20	−0.14	
$r_{11,12}$				+0.11	+0.40	
$r_{12,13}$					−0.23	
$r_{13,14}$					−0.25	

Table 7. Changes (in %) in bond lengths between the step atom and its nearest neighbours. The results from EAM are in parentheses.

Surface	SC–TC	SC–CC	SC–BNN	CC–BNN
Cu(211)	−1.78(−1.27)	−2.27(−2.67)	−3.22(−2.10)	+0.61(+0.7)
Cu(331)	−1.36(−0.45)	−2.39(−1.86)	−3.66(−3.09)	+1.42(+0.5)
Cu(511)	−1.80(−2.29)	−1.42(−0.98)	−3.13(−2.30)	+1.49(+1.5)
Cu(711)	−1.59(−2.16)	−1.36(−1.11)	−2.88(−2.26)	+1.06(+1.8)
Cu(911)	−1.22(−2.08)	−1.47(−1.06)	−3.06(−2.31)	+0.51(+1.93)

In figure 9 contour plots of the charge densities for Pd(211) surface are presented [54]. The plots have been drawn to give a cross sectional view of the plane passing through the step, the terrace corner and the BNN atoms. There is considerable charge redistribution near the step

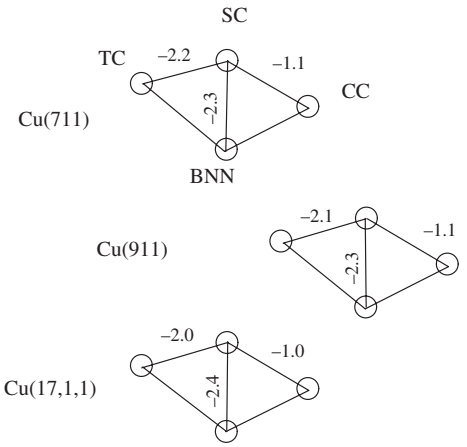

Figure 8. Bond length change between the step and its neighbours appears to be independent of the terrace width.

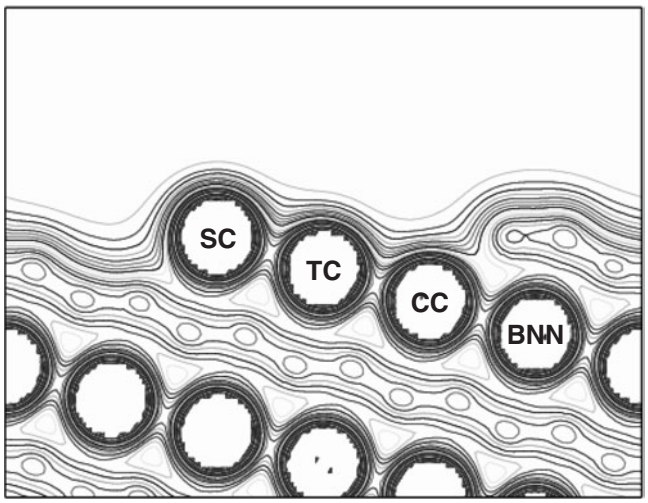

Figure 9. A cross sectional view of the changes in the electronic charge densities near steps.

edge and near the CC and BNN, but not near TC. The effect of the presence of the step is thus very much localized near the disturbance. For vicinals with larger terrace width than (211), the inhomogeneity due to the presence of steps would be even further localized to the step and corner atoms. The rest of the terrace atoms would behave just as on the mother surface, which in this case is Pd(111). The total electronic densities of states of the four regions of interest on Pd(211) [54] are displayed in figure 10. The reduced coordination of the step atom (SC) is reflected in the shift of the d-band centre towards the Fermi level and the narrowing of the density of states. The effect is much less on TC and CC and that of BNN is almost bulk like. It is reasonable to assume from discussions here that the electronic structural changes on vicinal surfaces are confined to local regions near the step and corner atoms.

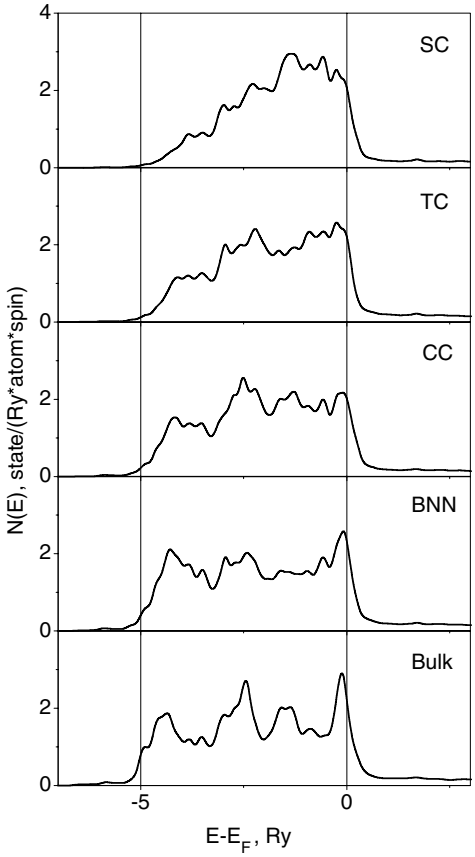

Figure 10. The layer resolved electronic density of states of Pd(211) determined by DFT-GGA calculations.

4.2. Changes in interatomic force constants

To appreciate the implications of multilayer relaxations of vicinal surfaces, we now turn to an examination of the force constant matrices associated with them. In tables 8–10 we present the force constant matrices $k_{\alpha\beta}$, where α and β stand for Cartesian components as obtained from EAM potentials between the SC atoms and their neighbours on the Cu(211), Cu(511) and Cu(331) surfaces, respectively. The force constants k_{xx} between the SC atoms in the direction perpendicular to the step, in the surface plane, are softened by 86% for Cu(211), 93% for Cu(511) and 85% for Cu(331), relative to their counterparts in the bulk, due to the loss of neighbours. This unpreventable softening causes the density of states for the step atom along the x direction to be shifted strongly to lower frequencies. Such softening in the force constant between SC atoms has also been reported for Ni(977) [4, 13] and for Au(511) [43]. The k_{zz} elements between SC and BNN atoms on Cu(211), Cu(511) and Cu(331) are, respectively, stiffened by 30, 35 and 45%. The stiffening of this force constant on Cu(331) and Cu(511) is obviously the reason for the strong contraction in their bond length. From the tables we also notice that the existence of steps on the surface induces changes not only in the diagonal elements of the force constant matrices of the surface atoms, but also in the off-diagonal elements. For example, k_{xz} and k_{yz} between SC and BNN atoms on Cu(511) are stiffened by

Table 8. Force constant matrices $k_{\alpha\beta}$ in (eV Å^{-2}/unit mass) for the interactions between the SC atom on Cu(511) and its nearest neighbours (on the surface and in the bulk).

		Surface			Bulk		
Atoms		x	y	z	x	y	z
	x	0.0057	0.0167	−0.0050	0.0887	0.0000	−0.0044
SC–SC	y	−0.0167	−1.6104	−0.2388	0.0000	1.9777	0.0000
	z	−0.0050	0.2388	0.0380	−0.0040	0.0000	0.1030
	x	−2.1859	0.0000	−0.8307	−1.8234	0.0000	−0.5452
SC–TC	y	0.0000	0.0678	0.0000	0.0000	0.0875	0.0000
	z	−0.3896	0.0000	−0.1067	−0.5452	0.0000	−0.0499
	x	−0.9416	−0.7116	0.6304	−0.8418	−0.7037	0.7594
CC–SC	y	−0.7637	−0.4282	0.4892	−0.7037	−0.4205	0.5598
	z	0.8832	0.6337	−0.5432	−0.7594	0.5598	−0.5238
	x	−0.0683	0.3926	−0.5996	−0.0769	0.3062	−0.4846
BNN–SC	y	0.3822	−0.5201	1.0726	0.3062	−0.4205	0.8454
	z	0.6337	1.1648	−1.7441	−0.4846	0.8454	−1.2888

30 and 35%, respectively. In table 11, we present the force constant matrices between two of the step atoms and between a step atom and a corner and a BNN atoms, for a relaxed surface of Ni(977) ('Surface') and the corresponding ones in the bulk ('Bulk'). Force constants are in eV Å^{-2}/unit mass. As seen from table 11, the reduction in the coordination results in a large softening of the force constant matrix elements between two steps atoms: 71% along x (k_{xx}) and 13.7 along y (k_{yy}), as compared to their counterparts in the bulk. Note that on Ni(111), k_{yy}, between neighbouring atoms in the top layer, is reduced by 5.7% from the bulk value. We also find a stiffening of 26% in the force constant between SC and CC atoms and of 17.2% in the force constant between SC and BNN atoms, both along the z direction (k_{zz}). Just as a softening in force constants tends to shift the frequencies toward lower values, a stiffening may lead to the creation of higher frequency modes which may appear above the bulk band or remain inside it as a resonant mode. In the following section we present the local vibrational density of states of the surface atoms of several vicinal surfaces and discuss the implications of the change in the force fields in the vicinity of the steps on the vibrational modes.

4.3. Local vibrational density of states

As an example, we present the calculated local density of states (LDOS) for the step and the terrace atoms of Ni(977) and compare them with those for the Ni(111) surface atoms in figure 11. It is interesting that the LDOS of the Ni(977) terrace atoms is very similar to that of Ni(111). This result suggests that in studies of phonons of vicinal surfaces with relatively large terraces, as in (977), or on realistic surfaces with non-regularly distributed steps, it is feasible to use a local approach to determine the phonons of the step and its surrounding atoms, while resorting to standard techniques for calculating phonons of the close packed flat surface for the terrace. Another interesting feature in figure 11 is that the low frequency modes associated with the step atoms display a global shift to lower frequencies, to the modes associated with the terrace (and Ni(111) surface atoms), thereby pointing to an extra softening of relevant force constants, in agreement with suggestions of Niu *et al* [4]. As we have seen in table 11, force constants between the surface atoms undergo both softening and stiffening.

In our work on Ni(977) [13], we have shown that the most prominent, low frequency mode is at 3.3 THz with maximum displacement along the x direction. For along the y and

Table 9. Force constant matrices $k_{\alpha\beta}$ in (eV Å^{-2}/unit mass) for the interactions between the SC atom on Cu(211) and its nearest neighbours (on the surface and in the bulk).

		Surface			Bulk		
Atoms		x	y	z	x	y	z
	x	0.0122	0.0613	0.0071	0.0931	0.0000	0.0079
SC–SC	y	−0.0613	−1.6129	−0.2330	0.0000	−1.9777	0.0000
	z	0.0071	0.2330	0.0008	0.0079	0.0000	0.0987
	x	−1.3793	0.8954	−0.6340	−1.2838	0.8500	−0.4907
SC–TC	y	0.8727	−0.4276	0.3859	0.8500	−0.4204	0.2932
	z	−0.3259	0.2036	−0.1298	−0.4907	0.2932	−0.0818
	x	−1.6344	0.0000	1.0355	−1.2837	0.0000	0.9814
CC–SC	y	0.0000	0.0898	0.0000	0.0000	0.0875	0.0000
	z	1.3683	0.0000	−0.7534	0.9814	0.0000	−0.5897
	x	0.1237	0.0162	−0.0582	0.0931	−0.0069	−0.0040
BNN–SC	y	−0.0140	−0.5070	1.1120	−0.0069	−0.4204	0.8991
	z	−0.0770	1.9530	−1.9071	−0.0040	0.8991	−1.4587

Table 10. Force constant matrices $k_{\alpha\beta}$ in (eV Å^{-2}/unit mass) for the interactions between the SC atom on Cu(331) and its nearest neighbours (on the surface and in the bulk).

		Surface			Bulk		
Atoms		x	y	z	x	y	z
	x	0.0149	0.0456	−0.0008	0.1034	0.0000	−0.0038
SC–SC	y	−0.0456	−1.6045	−0.2369	0.0000	−1.9777	0.0000
	z	−0.0008	0.2369	−0.0055	−0.0038	0.0000	0.0883
	x	−1.2389	−0.7979	−0.6305	−1.2436	−0.8310	−0.5361
SC–TC	y	−0.7815	−0.3905	0.3957	−0.8310	−0.4204	−0.3432
	z	−0.3288	−0.2154	−0.1622	−0.5361	−0.3432	−0.1220
	x	−0.6906	0.6684	0.7882	−0.5914	0.5903	0.7704
CC-SC	y	0.7191	−0.4868	−0.7498	0.5903	−0.4204	−0.6782
	z	−0.9997	−0.8795	−0.9733	0.7704	−0.6782	−0.7741
	x	−0.0153	0.0456	−0.7127	−0.0053	0.0000	−0.4649
BNN–SC	y	0.0000	0.1392	0.0000	0.0000	0.0875	0.0000
	z	−0.7140	0.0000	−2.7106	−0.4649	0.0000	−1.8681

z directions we found noticeable peaks, at low frequencies, at 3.9 and 4.9 THz, respectively. There was also a prominent high frequency peak at 9.1 THz, close to the top of the bulk band. The displacement vectors of the atoms for a mode at a given frequency were found from the imaginary part of the Green function. The polarization of the mode at 3.3 THz is shown in figure 12. Note that this mode is quasi-one dimensional: it involves only the concerted motion of the SC and CC atoms in conjunction with that of the TC atoms. The step atoms alternate with displacement vectors (+1, 0, −0.67) and (−1, 0, +0.67), the corner atoms with vectors (+0.27, 0, −1) and (−0.27, 0, +1) and the TC atoms with vectors (0, +0.24, 0) and (0, −0.24, 0). Thus the step and the corner atoms move in the xz plane, while the TC atoms move along the y direction to accommodate the propagation of this mode along the direction parallel to the step. The rest of the atoms are at rest. The wavelength of the mode is 2× *nearest neighbour distance* or 4.978 Å and its wavevector $q = (0.0, 1.262\ \text{Å}^{-1}, 0.0)$. This is a *super-*

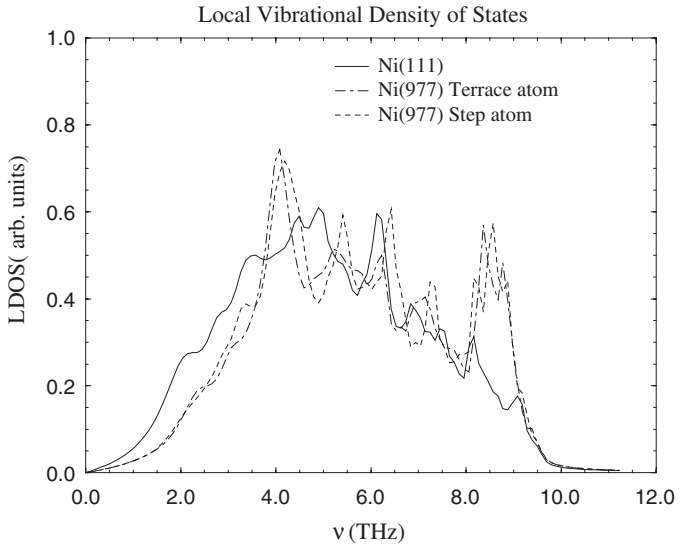

Figure 11. Projected vibrational densities of states for the Ni(977) step, terrace and Ni(111) surface atoms.

Table 11. Force constant matrices (in eV Å^{-2}/unit mass) between the step atom and it neighbours on Ni(977).

		Surface			Bulk		
Atoms		*x*	*y*	*z*	*x*	*y*	*z*
	x	0.0236	0.1489	0.0044	0.0816	0.0000	0.0058
SC–SC	*y*	−0.1489	−2.6386	−0.2796	0.0000	−3.0568	0.0000
	z	0.0044	0.2796	−0.0050	0.0058	0.0000	0.0805
	x	−1.5876	0.0000	1.7094	−1.3359	0.0000	1.5649
SC–CC	*y*	0.0000	0.0966	0.0000	0.0000	0.0753	0.0000
	z	2.0976	0.0000	−2.0658	1.5649	0.0000	−1.6342
	x	−0.0411	−0.3809	−0.6780	−0.0314	0.2890	−0.4983
SC–BNN	*y*	−0.3225	−0.7339	−1.5004	0.2890	−0.7026	1.3300
	z	−0.6080	−1.5720	−2.5342	−0.4983	1.3300	−2.1632

localized mode since the motion is restricted to the step atoms and their immediate neighbours on the surface. Modes like this exist on a number of vicinal surfaces. In table 12, we present a summary of the frequencies of the observed modes and refer the reader to discussions in related papers.

4.4. Vibrational free energies of vicinal surfaces

We now turn to a summary of the impact of undercoordination on the vibrational contribution to the thermodynamic properties of vicinal surfaces with a few specific examples. In figure 13, we show the vibrational LDOS for the step (SC), terrace (TC) and corner (CC) atoms of Cu(511), Cu(211) and Cu(331). The shift towards low frequencies, in each case, reflects the lower coordination of these atoms. There are some differences in LDOS between the sets of atoms on the three surfaces. On Cu(331), for example, the corner atom is almost bulk like while

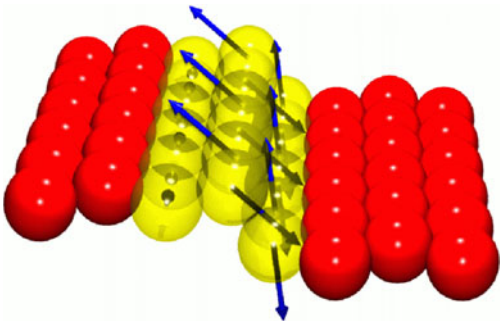

Figure 12. The displacement pattern of the step localized vibrational mode on Ni(977) (courtesy A Kara *et al*, JCP).

Table 12. Observed ('Exp.') and calculated ('Th.') vibrational modes on metal vicinal surfaces, in THz.

Surface	Method	Modes
Cu(511)	Exp. HAS [2]	1.51, 2.76, 3.24, 3.84
Cu(511)	Exp. EELS [3]	3.41
Cu(511)	Th. EAM-LD [3]	7.51, 7.80
Cu(511)	Th. EAM-RSGF [12]	2.25
Cu(511)	Th. EAM-LD [73]	1.1, 1.2, 1.6, 2.3, 2.8, 3.0, 3.25, 3.35, 6.4
Cu(211)	Exp. HAS [2]	1.32, 1.82, 2.52, 2.62, 2.66, 3.36
Cu(211)	Exp. EELS [3]	3.24, 8.16
Cu(211)	Th. EAM-LD [3]	2.35, 6.22, 7.51, 7.80
Cu(211)	Th. EAM-RSGF [12]	2.52
Cu(211)	Th. TB-LD[77]	2.50, 2.78, 3.25, 3.59, 6.20
Cu(211)	Th. DFT-PW [70]	2.76, 2.98, 5.93
Cu(211)	Th. EAM-LD [73]	1.2, 1.6, 2.3, 2.5, 2.8, 2.9, 3.3, 4.0, 4.2, 5.7, 6.3, 6.8
Cu(331)	Th. EAM-RSGF [12]	2.92, 5.26, 6.12
Cu(1,1,17)	Exp. EELS [3]	2.69, 3.14, 6.72
Cu(1,1,17)	Th. EAM-LD [3]	7.46, 7.92
Ni(977)	Exp. HAS [4]	3.55, 3.60
Ni(977)	Th. EAM-RSGF [13]	3.3, 3.9, 4.9, 9.1
Pt(775)	Exp. EELS [1]	6.15

the other two atoms contribute more to the lower frequency modes than the atoms in the bulk. As noted in previous publications [12, 55], the LDOS of the (211) and the (511) surfaces are similar to each other and different from those of the (331). These similarities and differences are related to trends in the multilayer relaxation patterns on these surfaces, as discussed above. Furthermore the plots in figure 13 suggest complexity in the way the different surface localities differ from those of the atoms in the bulk. We also find that the LDOS of the BNN atoms (in the layer adjacent to the corner atoms) show an enhancement in the *high* frequency region over bulk values [55]. This enhancement at the high frequency end is very prominent in the LDOS of the surface atoms on Cu(532) which has a regular array of kinks [56], as seen in figure 14.

The effect of the novelties in the vibrational dynamics is reflected in the calculated local vibrational free energy illustrated in figure 15 for the top layers of (511), (211) and (331). Atoms in all three surface chains (SC, TC, CC) are distinguished from the rest for (511) and (211). However for (331), layer 3 which corresponds to CC atoms on the terrace shows characteristics

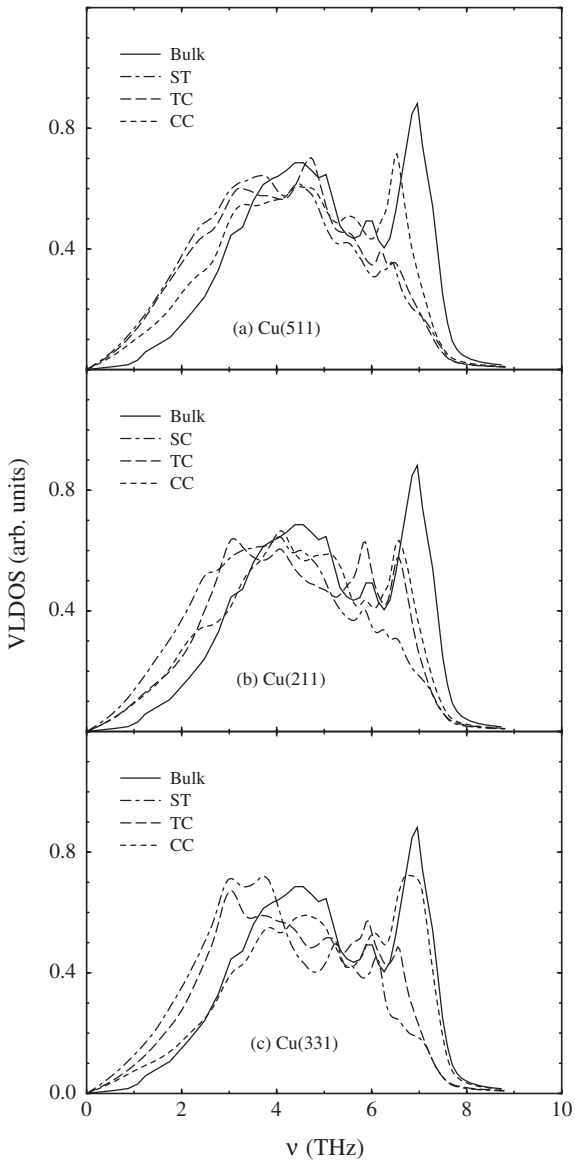

Figure 13. Projected vibrational densities of states of the step (SC), terrace (TC) and corner (CC) atoms on (a) Cu(511), (b) Cu(211) and (c) Cu(311) compared to that of a bulk atom.

more similar to those of a bulk atom than those of a surface atom. This interesting behaviour can again be traced to the effective coordination number. As we know from table 2, the coordination number for a CC atom of (511) and (211) is 10, while that of a (331) surface is 11, close to the value 12 for a bulk atom. During relaxation [12], while the CC atom of (211) and (511) moves upward, away from the bulk, that of (331) moves toward the rest of the bulk, increasing its effective coordination number. Note that the difference in coordination between the terrace atoms on (511) and (211) (8 and 9, respectively) is also displayed in the local free energies in figure 15. The terrace atoms on (511) have contributions closer to those

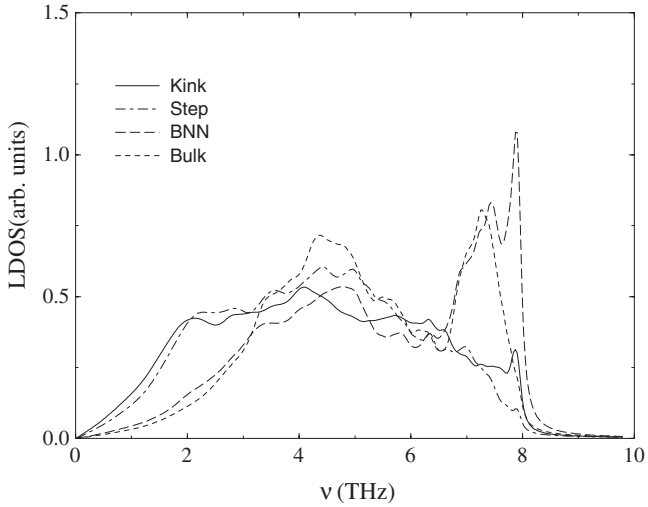

Figure 14. The projected vibrational density of states of kink sites on Cu(532).

of their step atoms, while on (211) they are closer to those of the corner atoms. In a recent publication [55], we have discussed in detail the effects of varying coordinations and complex relaxation patterns on the vibrational thermodynamic properties of the vicinal surfaces. We summarize the essential points here.

For convenience, we focus the discussion on the local quantities calculated at 300 K. Interestingly, the contributions of the step atoms (SC) are about the same on all three vicinal surfaces. On the Cu surfaces it is almost 41 meV/atom while on the Ag surfaces it is about 68 meV/atom. Although the percentage enhancement over the bulk value is significantly larger on Cu surfaces than on the Ag ones, in each case it is in excess of about 19 meV/atom over that in the bulk. Turning to the contributions of the TC atoms, we find a good correspondence with their respective coordinations. On (511) on which their coordination is 8, they contribute about 17 meV/atom more than the bulk atoms, similar to the value for the atoms on (100) surface with the same coordination. On (211) and (331), their contribution over the bulk is about 13–11 meV/atom, resembling that of the surface atoms on (111), which also have a coordination of 9. The largest difference in contribution for the atoms on the three types of vicinal surface comes from the corner atoms which on (331) contribute only 2–3 meV/atom more than the atoms in the bulk, while on (511) and (211) surfaces the corresponding amount is 9 meV/atom. This is again understandable from previous arguments based on atomic coordination. The atoms in the other layers in the tables have similar contributions to the bulk and small variations can again be linked to their relaxation and non-bulk-like contribution to the vibrational DOS. The above findings regarding the differential, local vibrational free energy contribution of atoms in undercoordinated sites show that the vibrational free energy does not scale with the coordination number in a simple manner, although its dependence on the coordination is remarkable. This is not surprising, as the coordination number is not the only factor controlling the characteristics. Relaxations of the individual atoms and their bond lengths with the surrounding atoms are also expected to play a role in defining local characteristics of a surface. Unlike those in flat surfaces, the atoms forming the terraces of vicinal surfaces experience a distinctive atomic environment because of the lack of symmetry along the direction perpendicular to the step edge, in the terrace plane, in addition to the

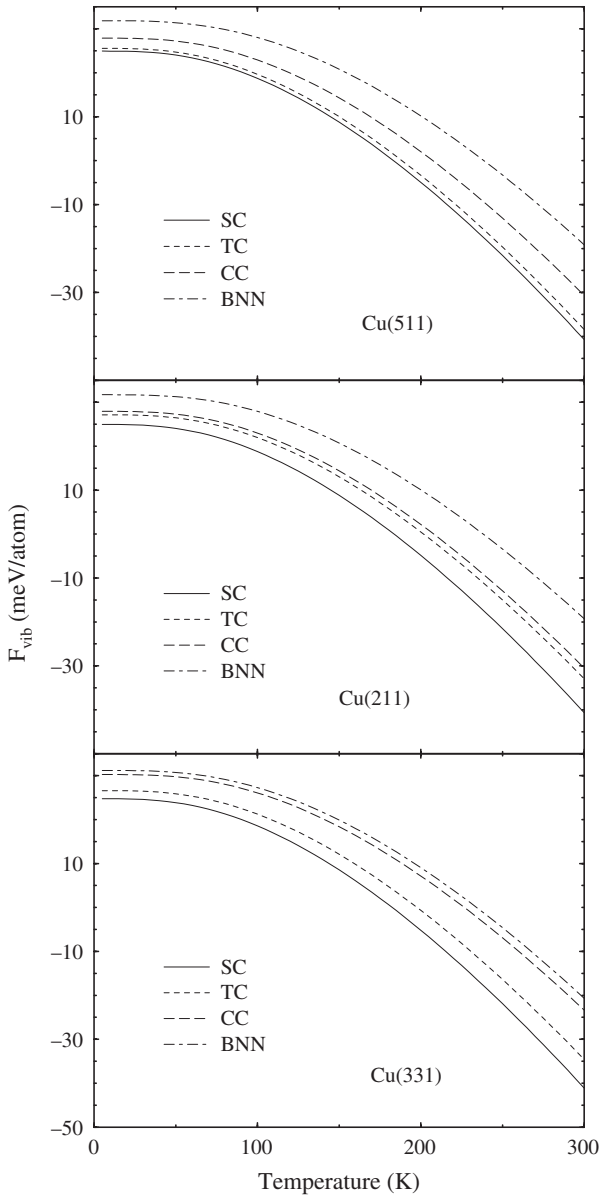

Figure 15. The dependence of the local contribution to the vibrational free energy of vicinal surfaces on the local coordination.

direction normal to it. This in turn leads to complex relaxation patterns and bond lengths for the surface atoms as shown in previous studies [12, 19], resulting in distinctive characteristics of the local regions on the surface.

Using the local contributions to the vibrational entropy we can calculate the surface and step excess free energies, following the procedure discussed earlier; we find the calculated surface excess vibrational free energies for Cu and Ag vicinals at 0, 100 and 300 K to be quite small. The calculation of the excess step free energies, however, shows a remarkable effect of

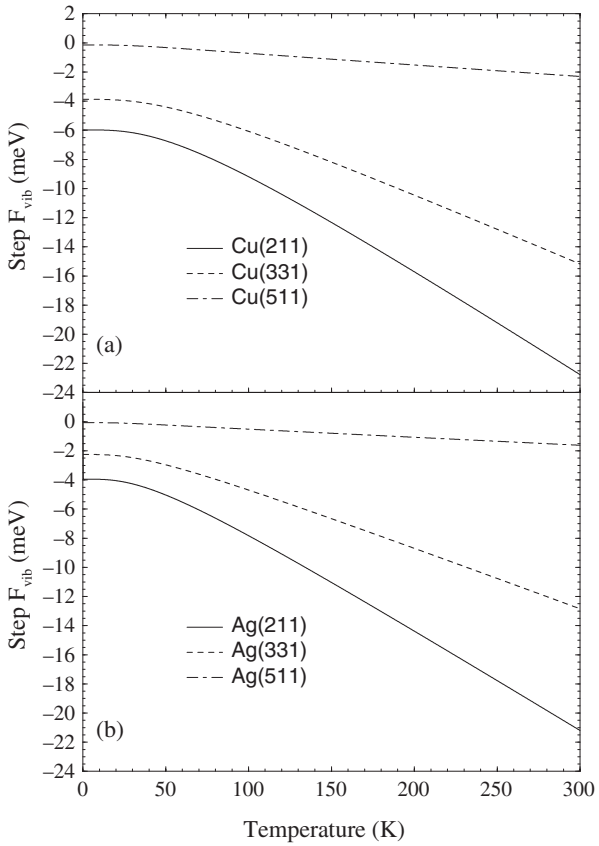

Figure 16. The dependence of the excess step free energy (vibrational part) on the surface geometry.

the vibrational component. The temperature variation of the step vibrational free energy for the three surface geometries is plotted in figure 16. It is remarkable that the excess vibrational contribution is almost non-existent for both Ag(511) and Cu(511). From 0 to 300 K it shows a variation of only 1 meV/atom. On the other hand, the contribution is remarkable for both Ag(211) and Cu(211) and constitutes about 10% of the total free energy [57] in the case of Cu. For Ag(211) it changes from −1.16 meV/atom at 0 K to −7.72 meV/atom at 300 K, while for Cu(211) it is −2.04 meV/atom at 0 K and −9.21 meV/atom at 300 K. The case of the (331) surfaces lies in between the other two geometries. For Ag(331) it decreases from 0 at 0 K to −2.93 meV/atom at 300 K and for Cu(331) it varies from −0.8 meV/atom at 0 K to −5.2 meV/atom at 300 K. Since the step free energy is relevant to the roughening temperature of a surface, we expect vibrational contributions to play an important role particularly for Cu(211) and Ag(211).

5. Summary

We have presented here a summary of the results of calculations of multilayer relaxations, selected dynamical properties and vibrational contributions to thermodynamic properties of a set of vicinal surfaces of several transition metals. Calculations were performed using either

ab initio electronic structure calculations or many body interaction potentials. Comparisons of results were made with available experimental data. The main conclusion to be drawn is that of the important role of the local coordination in determining the structural, dynamical and ultimately thermodynamical properties of these surface nanostructures. Of the large list of vicinals of varying surface geometry, terrace width, step face orientation and elemental metal studied here, the striking feature in the multilayer relaxation is the large outward relaxation of the corner atom (actually, the least undercoordinated atom) coupled with the inward relaxation of its neighbouring surface atom. While the inward relaxation of the step atom has been known of for a while, that of the 'corner' atom and its neighbour has been uncovered only recently. At least for Cu, Pd, Al and selected vicinals of Ni, Ag and Pt, the trends in the calculated multilayer relaxations point to this enhanced local effect at the step and near the corner site, in accordance with principles of charge smoothing. The reduced coordinations of the surface atoms lead to electronic densities of states which are narrow and shifted towards the Fermi level. Furthermore changes in the bond lengths of the surface atoms from their neighbours are reflected in corresponding softening and stiffening of force constants with respect to those in the bulk. As a result localized modes appear on stepped surfaces whose existence has been verified experimentally. Moreover projected vibrational densities of states of surface atoms show enhancements of modes at the low frequency end, as well as near (and sometimes above) the top of the bulk modes. The vibrational entropies of these surfaces are thereby impacted on by their local geometry and coordination. The local contributions scale with coordination in a complex manner. While the surface free energies of a set of vicinals of Ag and Cu show very little sensitivity to the vibrational contribution, the excess step free energy could have a vibrational contribution of about 25%.

In considerations of growth and surface stability, vibrational contributions cannot be ignored. Needless to say, surface relaxations are an inherent component of the novel features of vicinal surfaces and should not be ignored in any serious examination of these surfaces. Last but not least, the modifications in the structural, dynamical and subsequently thermodynamical properties introduced by the presence of steps on surfaces are local in nature, thereby allowing an extension of the knowledge gained from systematic studies of stepped surfaces to more complex environments such as those on nanocrystals.

Acknowledgments

This work was supported in part by the Basic Energy Research Division of the US Department of Energy Grant No DE-FG03-97ER45650 and by NSF–International Program for US–Turkey. We thank S Stolbov, C Ghosh and A Karim for help with figures and unpublished results.

References

[1] Ibach H and Bruchmann D 1978 *Phys. Rev. Lett.* **41** 958
[2] Witte G, Braun J, Lock A and Toennies J P 1995 *Phys. Rev.* B **52** 2165
[3] Kara A, Staikov P, Rahman T S, Radnik J, Biagi R and Ernst H J 2000 *Phys. Rev.* B **61** 5714
[4] Niu L, Gaspar D J and Sibener S J 1995 *Science* **268** 847
Niu L, Gaspar D J and Sibener S J 1995 *J. Chem. Phys.* **102** 9077
[5] For a review see Wandelt K 1991 *Surf. Sci.* **251/252** 387
[6] Hammer B 1999 *Phys. Rev. Lett.* **83** 3681
[7] Zambelli T, Wintterlin J, Trost J and Ertl G 1996 *Science* **273** 1688
[8] Gellman A, Horvath J D and Bülow M T 2001 *J. Mol. Catal.* A **167** 3
[9] Attard G A, Ahmadi A, Feliu J, Rodes A, Herrero E, Blais S and Jerkiewicz G 1999 *J. Phys. Chem.* B **103** 1381
[10] Lang B, Joyner R W and Somorjai A 1972 *Surf. Sci.* **30** 454

[11] Kara A, Durukanoğlu S and Rahman T S 1996 *Phys. Rev.* B **53** 15493
[12] Durukanoğlu S, Kara A and Rahman T S 1997 *Phys. Rev.* B **55** 13 894
[13] Kara A, Durukanoğlu S and Rahman T S 1997 *J. Chem. Phys.* **106** 2031
[14] Press W, Teukolsky S, Vetterling W and Flannery B 1992 *Numerical Recipes in Fortran* (Cambridge: Cambridge University Press)
[15] Foiles S M, Baskes M I and Daw M S 1986 *Phys. Rev.* B **33** 7983
Daw M S, Foiles S M and Baskes M I 1993 *Mater. Sci. Rep.* **9** 251
[16] Jacobsen K W, Norskov J K and Puska M J 1987 *Phys. Rev.* B **35** 7423
[17] Hohenberg P and Kohn W 1964 *Phys. Rev.* B **136** 864
[18] Perdew J P 1991 *Electronic Structure of Solids '91* ed P Ziesche and H Eschrig (Berlin: Academic)
[19] Heid R, Bohnen K P, Kara A and Rahman T S 2002 *Phys. Rev.* B **65** 115405
[20] Meyer B, Elsässer C and Fähnle M, *Fortran90 Program for Mixed-Basis Pseudopotential Calculations for Crystals* Max-Planck-Institut für Metallforschung, Stuttgart, unpublished
[21] Hedin L and Lundqvist B I 1971 *J. Phys. C: Solid State Phys.* **4** 2064
[22] Hamann D R, Schlueter M and Chiang C 1979 *Phys. Rev. Lett.* **43** 1494
Bachelet G B, Hamann D R and Schlüter M 1982 *Phys. Rev.* B **26** 4199
[23] Rodach Th, Bohnen K-P and Ho K M 1993 *Surf. Sci.* **286** 66
[24] Monkhorst H J and Pack J D 1976 *Phys. Rev.* B **13** 5188
[25] Kresse G and Hafner J 1993 *Phys. Rev.* B **47** 558
Kresse G and Furthmüller J 1996 *Comput. Mater. Sci.* **6** 15
Kresse G and Furthmüller J 1996 *Phys. Rev.* B **54** 11169
[26] http://www.fysik.dtu.dk/CAMP/dacapo.html
[27] Baroni S, Dal Corso A, de Gironcoli S and Giannozzi P http://www.pwscf.org
[28] Vanderbilt D 1990 *Phys. Rev.* B **41** 7892
[29] Makkonen I, Salo P, Alatalo M and Rahman T S 2003 *Phys. Rev.* B **67** 165415
[30] Kara A and Rahman T S 2003 to be published
[31] Spisak D 2001 *Surf. Sci.* **489** 151
[32] Lischka M and Groß A 2002 *Phys. Rev.* B **65** 075420
[33] Methfessel M and Paxton A T 1989 *Phys. Rev.* B **40** 3616
[34] Ercolessi F, Parrinello M and Tosatti E 1988 *Phil. Mag.* A **58** 213
[35] Finnis M W and Sinclair J E 1984 *Phil. Mag.* A **50** 45
[36] Yang L and Rahman T S 1991 *Phys. Rev. Lett.* **67** 2327
Yang L, Rahman T S and Daw M S 1991 *Phys. Rev.* B **44** 13725
Rahman T S 1994 *Condensed Matter Theories* vol 9 (New York: Nova Science) p 299
Al-Rawi A N, Kara A and Rahman T S 2000 *Surf. Sci.* **446** 17
[37] Tian Z J and Rahman T S 1993 *Phys. Rev.* B **47** 9751
[38] Kürpick U and Rahman T S 1997 *Surf. Sci.* **383** 137
[39] Stott M J and Zaremba E 1980 *Phys. Rev.* B **22** 1564
[40] Allen R E, Alldredge G P and de Wette F W 1971 *Phys. Rev.* B **4** 1648
[41] Haydock R, Heine V and Kelly M J 1972 *J. Phys. C: Solid State Phys.* **5** 2845
[42] Wu S Y, Cocks J and Jayanthi C S 1994 *Phys. Rev.* B **49** 7957
[43] Kara A, Jayanthi C S, Wu S Y and Ercolessi F 1994 *Phys. Rev. Lett.* **72** 2223
Kara A, Jayanthi C S, Wu S Y and Ercolessi F 1995 *Phys. Rev.* B **51** 17046
[44] Durukanoglu S and Rahman T S 2003 *Phys. Rev.* B **67** 205406
[45] Vitos L, Skriver H L and Kollar J 1999 *Surf. Sci.* **425** 212
[46] Jona F, Marcus P M, Zanazzi E and Maglietta M 1999 *Surf. Rev. Lett.* **6** 355
[47] Tian Y, Lin K W and Jona F 2000 *Phys. Rev.* B **62** 12844
[48] Smoluchowski R 1941 *Phys. Rev.* **60** 661
and see also Finnis M W and Heine V 1974 *J. Phys. F: Met. Phys.* **4** L37
[49] Allan G 1979 *Surf. Sci.* **89** 142
[50] Albrecht M, Blome R, Meyerheim H L, Moritz W and Robinson I K, unpublished
[51] Walko D A and Robinson I K 1999 *Phys. Rev.* B **59** 15446
[52] Walter S, Baier H, Weinelt M, Heinz K and Fauster Th 2001 *Phys. Rev.* B **63** 155407
[53] Durukanoglu S and Rahman T S 1998 *Surf. Sci.* **409** 395
[54] Stolbov S, unpublished
[55] Durukanoglu S, Kara A and Rahman T S 2003 *Phys. Rev.* B **67** 235405
[56] Kara A and Rahman T S 2003 to be published
[57] Feibelman P J 1999 *Phys. Rev.* B **60** 11118

[58] Watson P R and Mitchell K A R 1988 *Surf. Sci.* **203** 323
[59] Parkin S R, Watson P R, McFarlane R A and Mitchell K A R 1991 *Solid State Commun.* **78** 841
[60] Seyller Th, Diehl R D and Jona F 1999 *J. Vac. Sci. Technol.* A **17** 1635
[61] Tian Y, Lin K W and Jona F 2000 *Phys. Rev.* B **61** 4904
[62] Ismael, Chandravakar S and Zehner D M 2002 *Surf. Sci.* **504** L201
[63] Zhang X G, Van Hove M A, Somorjai G A, Rous P J, Tobin D, Gonis A, MacLaren J M, Heinz K, Michl M, Lindner H, Muller K, Ehsasi M and Block J H 1991 *Phys. Rev. Lett.* **67** 1298
[64] Adams D L, Jensen V, Sun X F and Vollesen J H 1988 *Phys. Rev.* B **38** 7913
[65] Noonam J R, Davis H L and Erley W 1985 *Surf. Sci.* **152/153** 142
[66] Adams D L and Sorensen C S 1986 *Surf. Sci.* **166** 495
[67] Adams D L, Moore W T and Mitchell K A R 1985 *Surf. Sci.* **149** 407
[68] Kolthoff D, Pfnur H, Fedorus A G, Koval V and Naumovets A G 1999 *Surf. Sci.* **439** 224
[69] Hirsimaki M, Pitkanen T, Lindroos M and Barnes C J 2000 *Surf. Sci.* **454–456** 6
[70] Wei C Y, Lewis S P, Mele E J and Rappe A M 1998 *Phys. Rev.* B **57** 10062
[71] Geng W T and Freeman A J 2001 *Phys. Rev.* B **64** 115401
[72] Nelson J S and Feibelman P J 1992 *Phys. Rev. Lett.* **68** 2188
[73] Sklyadneva I Yu, Rusina G G and Chulkov E V 1998 *Surf. Sci.* **416** 17
[74] Loisel B, Gorse D, Pontikis V and Lapujoulade J 1989 *Surf. Sci.* **221** 365
[75] Spangler J D, Kara A and Rahman T S 2003 to be published
[76] Kara A and Rahman T S 2003 to be published
[77] Raouafi F, Barreteau C, Spanjaard D and Desjonquères M C 2002 *Phys. Rev.* B **66** 045410